The importance of rare, high-wind events for dust uplift in northern Africa

Sophie M. Cowie[1], John H. Marsham[1], and Peter Knippertz[2]

[1]Institute for Climate and Atmospheric Science, School of Earth and Environment, University of Leeds, Leeds, UK, [2]Institute of Meteorology and Climate Research, Karlsruhe Institute of Technology, Karlsruhe, Germany

Abstract Dust uplift is a nonlinear thresholded function of wind speed and therefore particularly sensitive to the long tails of observed wind speed probability density functions. This suggests that a few rare high-wind events can contribute substantially to annual dust emission. Here we quantify the relative roles of different wind speeds to dust-generating winds using surface synoptic observations of dust emission and wind from northern Africa. The results show that winds between 2 and $5\,\mathrm{m\,s^{-1}}$ above the threshold cause the most emission. Of the dust-generating winds, 25% is produced by very rare events occurring only at 0.1 to 1.4% of the time, depending on the region. Dust-producing winds are underestimated in ERA-I, since it misses the long tail found in observations. ERA-I overpredicts (underpredicts) the frequency of emission strength winds in the southern (northern) regions. These problems cannot be solved by simple tunings. Finally, we show that rare events make the largest contribution to interannual variability in dust-generating winds and that ERA severely underestimates this interannual variability.

1. Introduction

Atmospheric mineral dust is an important component of the global climate system and is increasingly incorporated in weather and climate models. The Sahara and Sahel are the greatest contributors to the global dust budget [*Prospero et al.*, 2002; *Washington et al.*, 2003], but quantitative estimates of dust emission from northern Africa by global models vary by a factor of 5 or more [*Huneeus et al.*, 2011]. Uncertainty in land surface properties [*Menut et al.*, 2013] and modeled wind speeds [*Menut*, 2008; *Largeron et al.*, 2015] are known to be key sources of error, particularly in summer when models fail to capture the contribution from haboobs [*Marsham et al.*, 2011; *Heinold et al.*, 2013].

Dust emission occurs when the low-level wind generates a surface stress sufficient to exceed the threshold for dust emission [*Bagnold*, 1941], which depends on surface conditions of the soil [*Gillette et al.*, 1980]. This threshold can change significantly in relation to seasonal rainfall [*Cowie et al.*, 2014; hereafter CKM14]. Dust emission is commonly parameterized by a thresholded cubic function of friction velocity or near-surface wind speed [*Marticorena and Bergametti*, 1995]. The probability density function (pdf) of near-surface wind speed commonly follows a Weibull function, giving a skewed distribution with a long tail at high wind speeds [*Tuller and Brett*, 1984]. The highly nonlinear dependence of emission on wind, combined with the skewed pdf of near-surface wind speed, implies that few intense events can generate a significant climatological contribution to dust emission. For a 21 day record from the central Saharan Fennec supersite *Marsham et al.* [2013] noted that two high-wind-speed events contributed about 27% of total dust uplift. The possible disproportionate impact of this on the performance of global or regional dust models has not yet been systematically investigated for northern Africa.

To the best of our knowledge, this paper is the first to use long-term measurements of near-surface winds and eye observations of dust emission from the surface synoptic observation (SYNOP) network to quantify the impact of rare, high-wind events on climatological dust emission and interannual variability in northern Africa. The observational results are compared to ERA-Interim reanalysis data to reveal systematic deficiencies in model-dominated gridded wind products commonly used for offline or nudged dust simulations [*Menut*, 2008].

Section 2 describes the characteristics of the data used and the methods employed. Section 3 presents results of the climatological analysis and comparison to reanalysis data, while section 4 gives the main conclusions.
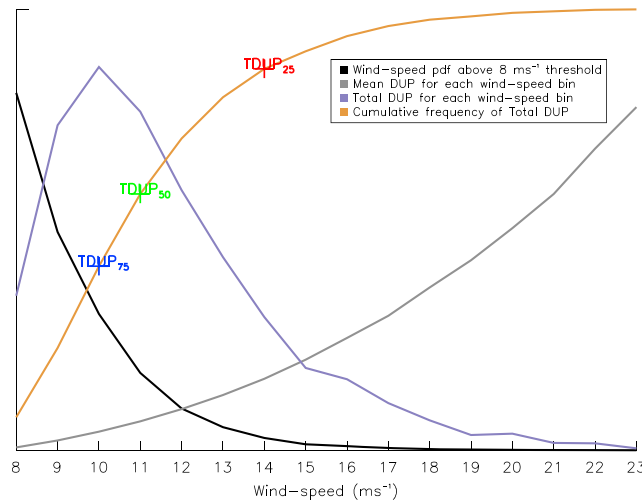
Figure 1. Illustration of the parameters calculated in order to determine TDUP$_{75}$, TDUP$_{50}$, and TDUP$_{25}$. Black line: tail of the wind speed pdf plotted in m s^{-1} bins; grey line: mean dust uplift potential (DUP) for each m s^{-1} bin; purple line: black line multiplied by grey line, the area below which gives the total DUP (TDUP); brown line: cumulative frequency of the TDUP line together with the points at which the curve reaches 0.25, 0.5, and 0.75 (TDUP$_{75}$, TDUP$_{50}$, and TDUP$_{25}$ wind speeds, respectively). See section 2.2.2 for further details. Note that no labeled axes are given for the sake of simplicity.

2. Methods and Data

2.1. Data

2.1.1. SYNOP Observations

This study uses long-term observations from 70 northern Africa stations, stored in the Met Office Integrated Data Archive System (MIDAS) SYNOP database for the period 1984–2012. Wind observations are made at 10 m height and 3- or 6-hourly intervals, for a 10 min mean period shortly before the synoptic hour and are in principle recorded at 1 knot (= 0.5 m/s) resolution. Eye observations by the station observer allow the identification of dust emission events via present weather codes (see CKM14 for details).

Although recorded at 1 knot intervals, for high winds some clustering of wind observations was noted around integer multiples of 10 knots (consistent with *DeGaetano* [1998] and *Cook* [2014]). This is likely a consequence of observers reading values from analogue anemometers, as still used in much of Africa, which have high wind speeds only marked at 10 knot intervals. This, alongside a small but ultimately unknown, number of missing reports due to reporting failure in severe weather, contributes to random, rather than systematic, error. If reports from the strongest dust storms are systematically missing, this will increase the importance of rare events and strengthen our conclusions.

Investigating the validity of high wind speeds from analogue anemometers, using METARs and the Spinning Enhanced Visible and Infrared Imager satellite imagery, found a plausible maximum value of 54 knots (see supporting information for details). Therefore, if not noted otherwise, only values <55 knots were used in our analysis. Above threshold winds not accompanied by a dust emission report are also excluded, as these instances indicate possible observer-reporting errors (typographic errors were found after detailed investigation, see supporting information Text S1). For better presentation and statistical robustness, stations are grouped together and averaged using the six regions as defined in CKM14 (see Figure S1).

2.1.2. ERA-Interim Reanalysis Data

Ten meter u and v surface winds from the European Centre for Medium-Range Weather Forecasts ERA-Interim reanalysis data set (ERA-I herein) [*Dee et al.*, 2011] are extracted for the grid point nearest to each observation station. To compare directly with observations, a 3-hourly resolution is achieved by extracting the analysis products at 0000 and 1200 UTC and the associated +3 h, +6 h, and +9 h short-term forecasts. Only the times with an equivalent observation are extracted to account for biases and gaps in the observational record. Each grid box is representative of an 80 km × 80 km area over a station. We compare these grid box mean winds, which do not include a contribution from turbulence, with observations that do and expect that the 10 min averaging applied to observations will remove much of the turbulent contribution. The data are further subsampled to times when there is a dust emission report above the threshold and all reports (dust emission or not) below the threshold (see section 2.2.1 for details on thresholds).

2.2. Methods

2.2.1. Dust Uplift Potential

In the absence of quantitative information on dust uplift *Marsham et al.* [2011] proposed to measure the dust-emitting "power" of the wind with a dust uplift potential (DUP) based on the emission parameterization initially created by *White* [1979] and adapted from *Marticorena and Bergametti* [1995]:

$$\text{DUP} = U^3(1 + U_t/U)(1 - U_t^2/U^2) \qquad \text{for } U > U_t \qquad (\text{and } 0 \text{ otherwise}),$$
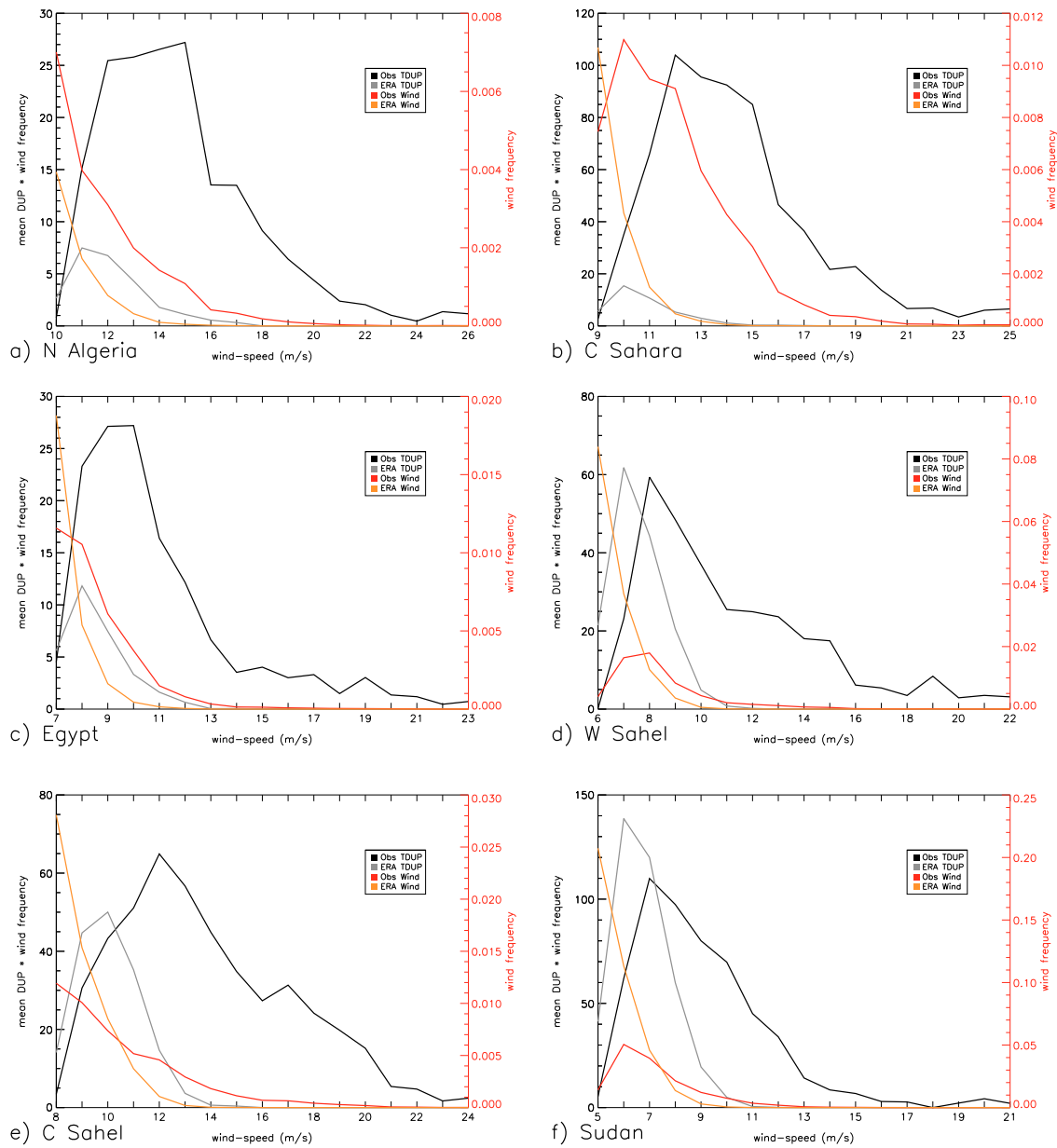
Figure 2. Total DUP and wind speed probability functions for dust-only observations (black and red) and ERA-I (grey and orange), using the region-dependent thresholds defined in CKM14. The method used to calculate the black and grey lines is explained in section 2.2.2. Note the different axes. The definition of regions is shown in Figure S1 in the supporting information.

where U is the 10 m wind speed and U_t is a threshold for dust emission. For a site in the central Sahara, *Marsham et al.* [2013] showed that variations in DUP are closely tied to variations in low-level dustiness, when dustiness is dominated by fresh emission rather than transported dust. For the Sahel, where the land surface changes with time, seasonal variations in dust emission are a function of land surface change, as well as DUP. DUP is therefore a valuable means to study the variation in wind speed relevant to dust uplift and can isolate the role of meteorology from that of the land surface.

Calculating DUP requires a threshold U_t. The thresholds used here are the T_{25} values from CKM14, where T_{25} is the wind speeds at which 25% of all reports (which contained a wind observation) also made a dust emission report simultaneously. These values range from 5 m s^{-1} in Sudan to 10 m s^{-1} in Algeria (Table S2 in the supporting information).
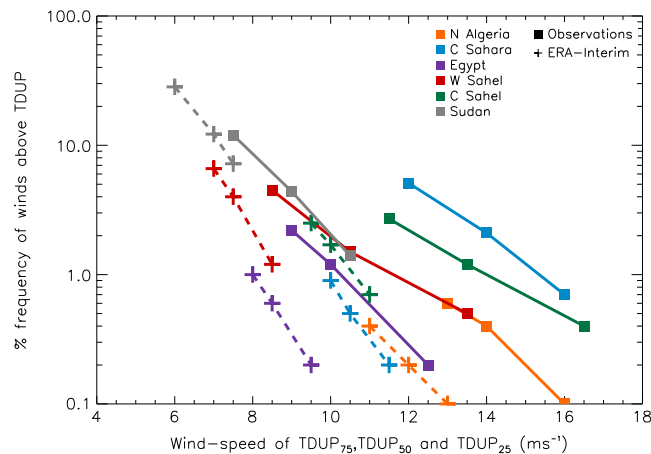
Figure 3. $TDUP_{75}$, $TDUP_{50}$, and $TDUP_{25}$ (from left to right for each set of three plotted points) against the frequency of occurrence of winds above TDUP (plotted on a log scale) for each of the six regions in northern Africa, as defined in CMK14. ERA-I is denoted by dashed lines and crosses, observations by solid lines and squares.

2.2.2. Probability Density Functions of Wind Speed and DUP

Wind speeds and DUP are analyzed here using pdfs and cumulative frequency curves as schematically illustrated in Figure 1. First, a pdf of wind speed with an integral area of 1 is calculated. For many stations this pdf follows a typical Weibull distribution. In Figure 1 only the part of the pdf over the emission threshold (an arbitrary $8\,m\,s^{-1}$) is shown. Then DUP is calculated for each wind speed bin (grey line, Figure 1), reflecting the cubic dependence on wind speed. Multiplying this curve with the wind pdf gives a distribution of DUP, whose integral area is equal to the total DUP (TDUP; blue line in Figure 1). Where the TDUP cumulative frequency curve (brown; Figure 1) exceeds 0.5 is, the wind speed above which 50% of total DUP occurs. Wind speeds above which 75% and 25% of the total DUP occurs are also computed similarly to give the three terms $TDUP_{75}$, $TDUP_{50}$, and $TDUP_{25}$ (marked in blue, green, and red in Figure 1).

3. Results and Discussion

3.1. Contribution of Different Wind Speeds to Dust-Generating Winds

Analogous to Figure 1, Figure 2 presents pdfs of wind speed exceeding the T_{25} threshold and curves of TDUP computed from SYNOPs in each of the six regions (red and black lines, respectively). In N Algeria, Egypt, and C Sahel the wind pdf tails have a Weibull-like shape which drops steadily from the threshold. In the other three regions, the wind pdfs show a secondary maximum 1 or $2\,m\,s^{1}$ above the threshold (Figures 2b, 2d, and 2f). This is because only wind reports accompanied by dust emission reports are considered, which peak above T_{25} in these three regions. Despite these differences, the resulting TDUP curves show quite similar shapes (in agreement with Figure 1). Maximum TDUP occurs anywhere from 2 to $5\,m\,s^{-1}$ above the threshold with the narrowest shapes in the regions with lowest thresholds (Egypt, W Sahel, and Sudan) and the widest shape in N Algeria, where the wind speed corresponding to the TDUP maximum is $15\,m\,s^{-1}$ (Figure 2a).

The $TDUP_{75}$, $TDUP_{50}$, and $TDUP_{25}$ (left to right for each set of three points in Figure 3) wind speeds are plotted on the x axis against the frequency of occurrence of winds over that TDUP wind speed (y axis, Figure 3). Twenty-five percent of total DUP is caused by winds exceeding $10.5-16\,m\,s^{-1}$ (far right square for each set of three points plotted in Figure 3). Such winds occur between 0.1% (N Algeria) and 1.4% (Sudan) of the time. Assuming a complete set of 3-hourly SYNOP reports, 0.1% corresponds to only three reports per year. In other words, one dust storm lasting for just over 6 h could cause a quarter of the annual dust output in this region, where the observed mean dust emission frequency is 2% (Table S2 in the supporting information). The high mean emission frequency of 27% in Sudan (Table S2 in the supporting information) is reasonable given that *Allen et al.* [2015] found the frequency of emission at Bordj-Badji Mokhtar to be 22% in June 2011 and 28–33% in June 2012. Sensitivity of these results was tested by (a) normalizing the data, (b) including all data (those over 55 knots), (c) using different group-averaging methods, and (d) using different emission thresholds. Results were found to be relatively insensitive to (a)–(c) and most sensitive to (d) (supporting information).

3.2. Comparison With ERA-Interim 10 m Winds

The equivalent results for ERA-Interim data, temporally sampled to available station observations, are given in orange and grey lines in Figure 2 and the dashed lines with crosses in Figure 3. In all regions, ERA-I winds drop off substantially more quickly than the observed curves (orange versus red curves in Figure 2). This leads to narrower TDUP distributions shifted to lower values and, with the exception of W Sahel and Sudan, also to

Table 1. Total Integrated DUP and Percentage Total Integrated DUP Over the Six Regional Groups of Observation Stations[a]

Region	Observations TIDUP (Freqency of Occurrence)	ERA TIDUP	ERA Using $T_{25}-1$	ERA Using $T_{25}-2$	(ERA /Obs) × 100	(ERA $T_{25}-1$ /Obs) × 100	(ERA $T_{25}-2$ /Obs) × 100
N Algeria	177(0.4)	25(0.2)	48(0.4)	85(0.6)	14	27	48
C Sahara	654(2.1)	42(0.5)	93(0.9)	184(1.6)	6	14	28
Egypt	142(1.2)	31(0.6)	73(1.7)	147(3.4)	22	51	104
W Sahel	317(1.5)	154(4)	290(6.1)	452(11.5)	49	91	143
C Sahel	468(1.2)	163(1.7)	272(2.4)	399(3.8)	35	58	85
Sudan	561(4.4)	385(12.2)	654(20.4)	916(37.2)	69	117	163

[a]Total Integrated TDUP (TIDUP) uses the T_{25} threshold for each region, and additionally $T_{25}-1$ and $T_{25}-2$ for ERA-I. The last three columns are the percentage TIDUP calculated as (ERA TIDUP/Obs TIDUP) × 100.

lower peak values (black versus grey curves in Figure 2). The TDUP distributions in ERA-I all have a much smaller contribution from their tail at high wind speeds, due to the less frequent occurrence of high winds in ERA-I compared with observations.

The larger differences between ERA-I and observations in the top part of the wind distribution are reflected in Figure 3 by much larger deviations in $TDUP_{25}$ (far right squares and crosses 3–5 m s^{-1}) compared to those in $TDUP_{75}$ (far left squares and crosses 1–2 m s^{-1}). Overall, the differences are smallest in Egypt and largest in the C Sahel. In Egypt, a larger proportion of observed TDUP occurs close to the threshold, and despite its long tail, the contribution from those highest winds is not large. In other regions the tail is a bigger contributor to DUP and therefore the differences in $TDUP_{25}$ between observations and ERA-I are larger.

Although ERA-I produces lower TDUP values across all regions (Figure 3), the pattern for differences in frequency of occurrence differs from northern (N Algeria, C Sahara, and Egypt) to southern (W Sahel, C Sahel, and Sudan) regions. In the north, frequency of occurrence of dust-emitting winds is less, despite the lower TDUP thresholds used to calculate the values. This can be seen in the pdfs of Figure 2, where the ERA-I pdf line is always below the observational pdf line (orange and red, respectively). In the south, ERA-I more frequently produces winds over the lower TDUP thresholds (grey, red, and green dashed in Figure 3). Correspondingly, in Figure 2 we see an overprediction close to the threshold by ERA-I and that this overprediction overcompensates for the missing tail (orange line, Figure 2).

The regional variations in the biases of ERA-I compared with observations shown in Figure 3 reveal that tuning a dust model using ERA-I winds to give the correct total dust emission will not give the correct frequency of occurrence of dust emission or the correct relative contributions from different wind speeds. Lowering ERA-I thresholds is a physically justifiable approach as emission is expected to occur when the ERA-I grid box-mean wind is lower than the threshold estimated from station data, due to subgrid variations in wind speed.

To explore a tuning by lowering thresholds in ERA-I, the total integrated DUP (TIDUP) and frequency of occurrence at $TDUP_{50}$ statistics are calculated for observations using the T_{25} threshold (Table 1, column 2) and compared to ERA-I values using the same threshold (Table 1, column 3) and then with $T_{25}-1$ m s^{-1} and -2 m s^{-1} (Table 1, columns 4 and 5) to see if these lower thresholds can improve the TIDUP and frequency of events statistics. ERA-I always falls short in TIDUP, predicting between 6 to 69% of the observed value (Table 1, column 6). However, at this T_{25} threshold the frequency of events in ERA-I is already too high in the three southern regions. Lowering the threshold in any of these regions only enhances this discrepancy (Table 1, rows 5–7 and columns 2–5). In the three northern regions, however, decreasing the threshold does improve ERA-I frequency of events, although the effect depends regionally on how much you decrease the threshold. N Algeria only needs a 1 m s^{-1} decrease, while in C Sahara a 2 m s^{-1} decrease is still too low to fully reach observed frequency of occurrence and TIDUP. In Egypt, $T_{25}-1$ m s^{-1} increases TIDUP from 22% to 51% of observed TIDUP, but increases the frequency of occurrence to 1.7%, which is 0.5% above the observations level. Overall, this means that lowering emission thresholds could slightly improve predictions of dust emission in C Sahara (if lowered more than 2 m s^{-1}), but elsewhere, lowering (or increasing) the thresholds would disrupt the balance of the frequency of events and the total amount of dust uplift.

3.3. Interannual Variability of Dust-Generating Winds

Section 3.1 shows how rare events make a substantial contribution to the dust-generating power of the winds (DUP) in all areas. It is therefore interesting to see how much these rare events contribute to interannual

Table 2. Largest Contributors from the TDUP Distribution to Interannual Variability in ERA and Observations and Correlations Between Observations and ERA DUP Time Series[a]

	N Algeria	C Sahara	Egypt	W Sahel	C Sahel	Sudan
Obs (T_{25} threshold)	25+	25+	25+	100–75	25+	25+
ERA (T_{25} threshold)	25+	50–25	50-25	75–50	25+	25+
ERA (T_{25}−1 threshold)	25+	75–50	25+	25+	50-25	25+
ERA (T_{25}−2 threshold)	25+	25+	100-75	25+	25+	25+
Correlation ERA-I T_{25}−2 with Obs time series	**0.5**	**0.5**	0.1	**0.4**	−0.1	**0.5**
Correlation ERA-I T_{25} with Obs time series	**0.5**	0.3	0	0.3	0	**0.4**

[a]The values 25, 50, etc. are the wind speeds above which 25%, 50%, etc. of the total dust uplift occurs. For example, 75–50 is the contribution of winds that are over the TDUP_{75} wind speed, but below TDUP_{50}. The last two rows give the correlation of annually averaged TDUP for ERA-I (using T_{25}−2, T_{25}) and Observations (using T_{25}). Bold italics indicate >99% significant and just bold >95%.

variations in DUP. These could be tied to single synoptic-scale weather events such as Mediterranean cyclones [*Alpert and Ziv*, 1989; *Trigo et al.*, 1999] or to some longer-lasting identifiable meteorological regime, as, for example, a shift of the Azores High into northwestern Africa or a strengthening of the Libyan High [*Knippertz*, 2014].

Here we use an analysis of variance for the detrended time series of mean annual DUP for each of the six regions, with the total DUP split into four wind speed subsets from winds between (1) DUP threshold to TDUP_{75}, (2) TDUP_{75} to TDUP_{50}, (3) TDUP_{50} to TDUP_{25}, and (4) greater than TDUP_{25}+. These four contributions from increasing winds are assigned the letters K, X, Y, and Z, respectively. The variance sum law for correlated variables,

$$\text{Var}\left(\sum_{i=1}^{n} X_i\right) = \sum_{i=1}^{n}\text{Var}(X_i) + 2\sum_{1\le i}\sum_{<j\le n}\text{Cov}(X_i, X_j),$$

is expanded to include the four DUP time series

$$\text{Var}(K + X + Y + Z) = \text{Var}(K) + \text{Var}(X) + \text{Var}(Y) + \text{Var}(Z)$$

$$+ 2(\text{cov}(K, X) + \text{cov}(K, Y) + \text{cov}(K, Z)$$

$$+ \text{cov}(X, Y) + \text{cov}(X, Z)) + \text{cov}(Y, Z))$$

to find the total contribution to interannual variations in DUP from each subset of winds that the variance and covariance terms that contain that term are summed. For the example of TDUP_{75}–TDUP_{50} (x), the contribution is calculated by

$$\text{contribution}(X) = \text{Var}(X) + \text{cov}(K, X), + \text{cov}(X, Y) + \text{cov}(X, Z)$$

The rarest wind speeds (those in the TDUP_{25} + subset) contribute the most to total variance in all regions except W Sahel (Table 2, row 1). In N Algeria, C Sahara, and C Sahel all the covariance terms are positive, indicating that all the dust events of various wind speeds are positively correlated with each other. Elsewhere, this was not the case, with at least one negative covariance between subsets within those regions. This could be a signal of different mechanisms producing different strengths of dusty winds, operating on different time scales. The time series variance is much higher in observations than in ERA-I, ranging from a factor of 4 in N Algeria to 64 in C Sahel.

The detrended time series of mean annual DUP from ERA-I and observations have correlations ranging regionally from 0 to 0.5 (Table 2, row 6). Such low correlations from analyses likely help explain why Coupled Model Intercomparison Project models struggle to capture past interannual variability in dustiness [*Evan et al.*, 2014]. If ERA-I is "tuned" by decreasing the threshold by $2\,\text{m\,s}^{-1}$ (T_{25}−2), four of the six regions attribute most of the variability to the rarest events in the 25+ category of wind speed (Table 2, rows 1 and 4). The interannual variability correlations (Table 2, rows 5 and 6) are also improved slightly, though still low overall. However, as discussed in section 3.2, lowering thresholds alone will not necessarily improve the agreement of ERA with observations and should be approached with caution.

4. Conclusions

The relative roles of different wind speeds to dust uplift potential (DUP) and its interannual variability was investigated over six regions in northern Africa using long-term surface SYNOP observations. Results from this analysis were compared to ERA-I reanalysis data. Sensitivity studies that support the main conclusions are robust to changing data quality criteria, thresholds, and averaging methods.

1. Overall observed dust emission occurrence frequency varies widely between regions (2 to 27% for N Algeria and Sudan, respectively). Winds from 2 to $5\,\mathrm{m\,s^{-1}}$ above the threshold contribute most to the dust-generating wind. The largest contributions are from winds ranging from $7\,\mathrm{m\,s^{-1}}$ (Sudan) to $15\,\mathrm{m\,s^{-1}}$ (N Algeria).
2. Twenty-five percent of DUP results from events that only occur between 0.1% and 1.4% of the time, which equates to only 0.4 to 5 d/yr.
3. Wind speeds from reanalysis showed a pdf with a stunted tail, which omits the high wind speeds found in observations. ERA-I TDUP events occur 1 to 5 times too frequently in southern regions and 1 to 5 times too infrequently in northern regions.
4. Rare high-wind events that produce 25% of the total DUP contribute the most to interannual variability for the time period 1984–2012 in five of the six regions. Correlations only reach 0.5 between ERA-I and observations, even with lowered ERA thresholds.

This work demonstrates the importance of rare high-wind events over northern Africa for dust uplift. The quantified differences between ERA-I and observations in both wind-generated uplift and frequency of events that produce this uplift show that ERA-I cannot reproduce observed dust emission by a simple tuning such as lowering emission threshold. It supports the use of more complex approaches than simply using ERA-I grid-scale winds for dust emission modeling, e.g., accounting for subgrid variations in winds and missing processes such as haboobs [*Cakmur et al.*, 2004; *Pantillon et al.*, 2015].

References

Allen, C. J., R. Washington, and A. Saci (2015), Dust detection from ground-based observations in the summer global dust maximum: Results from Fennec 2011 and 2012 and implications for modeling and field observations, *J. Geophys. Res. Atmos.*, *120*, 897–916, doi:10.1002/2014JD022655.

Alpert, P., and B. Ziv (1989), The Sharav cyclone: Observations and some theoretical considerations, *J. Geophys. Res.*, *94*(D15), 18,495–18,514, doi:10.1029/JD094iD15p18495.

Bagnold, R. A. (1941), *The Physics of Blown Sand and Desert Dunes*, 265 pp., Methuen, London.

Cakmur, R. V., R. L. Miller, and O. Torres (2004), Incorporating the effect of small-scale circulations upon dust emission in an atmospheric general circulation model, *J. Geophys. Res.*, *109*, D07201, doi:10.1029/2003JD004067.

Cook, N. J. (2014), Review of errors in archived wind data, *Weather*, *69*(3), 72–78.

Cowie, S. M., P. Knippertz, and J. H. Marsham (2014), A climatology of dust emission events from northern Africa using long-term surface observations, *Atmos. Chem. Phys.*, *14*(16), 8579–8597, doi:10.5194/acp-14-8579-2014.

Dee, D. P., et al. (2011), The ERA-Interim reanalysis: Configuration and performance of the data assimilation system, *Q. J. R. Meteorol. Soc.*, *137*, 553–597, doi:10.1002/qj.828.

DeGaetano, A. T. (1998), Identification and implications of biases in U.S. surface wind observation, archival, and summarization methods, *Theor. Appl. Climatol.*, *60*(1–4), 151–162, doi:10.1007/s007040050040.

Evan, A. T., C. Flamant, S. Fiedler, and O. Doherty (2014), An analysis of aeolian dust in climate models, *Geophys. Res. Lett.*, *41*, 5996–6001, doi:10.1002/2014GL060545.

Gillette, D. A., J. Adams, A. Endo, D. Smith, and R. Kihl (1980), Threshold velocities for input of soil particles into the air by desert soils, *J. Geophys. Res.*, *85*(C10), 5621–5630, doi:10.1029/JC085iC10p05621.

Heinold, B., P. Knippertz, J. H. Marsham, S. Fiedler, N. S. Dixon, K. Schepanski, B. Laurent, and I. Tegen (2013), The role of deep convection and nocturnal low-level jets for dust emission in summertime West Africa: Estimates from convection-permitting simulations, *J. Geophys. Res. Atmos.*, *118*, 4385–4400, doi:10.1002/jgrd.50402.

Huneeus, N., et al. (2011), Global dust model intercomparison in AeroCom phase I, *Atmos. Chem. Phys.*, *11*(15), 23,781–23,864, doi:10.5194/acp-11-7781-2011.

Knippertz, P. (2014), Meteorological aspects of dust storms, in *Mineral Dust: A Key Player in the Earth System*, edited by P. Knippertz and J.-B. W. Stuut, pp. 121–148, Springer, Netherlands.

Largeron, Y., F. Guichard, D. Bouniol, F. Couvreux, L. Kergoat, and B. Marticorena (2015), Can we use surface wind fields from meteorological reanalyses for Sahelian dust emission simulations?, *Geophys. Res. Lett.*, *42*, 2490–2499, doi:10.1002/2014GL062938.

Marsham, J. H., P. Knippertz, N. S. Dixon, D. J. Parker, and G. M. S. Lister (2011), The importance of the representation of deep convection for modeled dust-generating winds over West Africa during summer, *Geophys. Res. Lett.*, *38*, L16803, doi:10.1029/2011GL048368.

Marsham, J. H., et al. (2013), Meteorology and dust in the central Sahara: Observations from Fennec supersite-1 during the June 2011 intensive observation period, *J. Geophys. Res. Atmos.*, *118*, 4069–4089, doi:10.1002/jgrd.50211.

Marticorena, B., and G. Bergametti (1995), Modeling the atmospheric dust cycle: 1. Design of a soil-derived dust emission scheme, *J. Geophys. Res.*, *100*, 16,415–16,430, doi:10.1029/95JD00690.

Menut, L. (2008), Sensitivity of hourly Saharan dust emissions to NCEP and ECMWF modeled wind speed, *J. Geophys. Res.*, *113*, D16201, doi:10.1029/2007JD009522.

Menut, L., C. Pérez, K. Haustein, B. Bessagnet, C. Prigent, and S. Alfaro (2013), Impact of surface roughness and soil texture on mineral dust emission fluxes modeling, *J. Geophys. Res. Atmos.*, *118*, 6505–6520, doi:10.1002/jgrd.50313.

Pantillon, F., P. Knippertz, J. Marsham, and C. Birch (2015), A parameterization of convective dust storms for models with mass-flux convection schemes, *J. Atmos. Sci.*, *72*, 2545–2561, doi:10.1175/JAS-D-14-0341.1.

Prospero, J. M., P. Ginoux, O. Torres, S. E. Nicholson, and T. E. Gill (2002), Environmental characterization of global sources of atmospheric soil dust identified with the Nimbus 7 Total Ozone Mapping Spectrometer (TOMS) absorbing aerosol product, *Rev. Geophys.*, *40*(1), 1002, doi:10.1029/2000RG000095.

Trigo, I. F., T. D. Davies, and G. R. Bigg (1999), Objective climatology of cyclones in the Mediterranean region, *J. Clim.*, *12*(6), 1685–1696, doi:10.1175/1520-0442(1999)012<1685:OCOCIT>2.0.CO;2.

Tuller, S. E., and A. C. Brett (1984), The characteristics of wind velocity that favor the fitting of a Weibull distribution in wind speed analysis, *J. Climate Appl. Meteorol.*, *23*(1), 124–134, doi:10.1175/1520-0450(1984)023<0124:TCOWVT>2.0.CO;2.

Washington, R., M. Todd, N. J. Middleton, and A. S. Goudie (2003), Dust-storm source areas determined by the total ozone monitoring spectrometer and surface observations, *Ann. Assoc. Am. Geogr.*, *93*(2), 297–313, doi:10.1111/1467-8306.9302003.

White, B. R. (1979), Soil transport by winds on Mars, *J. Geophys. Res.*, *84*(B8), 4643–4651, doi:10.1029/JB084iB09p04643.